Research Article

Combined system identification and robust control of a gimbal platform

Mehmet BASKIN[1,*] , **Kemal LEBLEBİCİOĞLU**[2]

[1]Aselsan Inc., Ankara, Turkey

[2]Department of Electrical-Electronics Engineering, Middle East Technical University, Ankara, Turkey

Abstract: Gimbaled imaging systems require very high performance inertial stabilization loops to achieve clear image acquisition, precise pointing, and tracking performance. Therefore, higher bandwidths become essential to meet recent increased performance demands. However, such systems often posses flexible dynamics around target bandwidth and time delay of gyroscope sensors which put certain limit to achievable bandwidths. For inertial stabilization loops, widely used design techniques have difficulty in achieving large bandwidth and satisfying required robustness simultaneously. Clearly, high performance control design hinges on accurate control-relevant model set. For that reason, combined system identification and robust control method is preferred. In the system identification step, accurate nominal model is obtained, which is suitable for subsequent robust control synthesis. Model validation based uncertainty modeling procedure constructs the robust-control-relevant uncertain model set, which facilitates the high performance controller design. Later, with skewed-μ synthesis, controller is designed which satisfies large bandwidth and robustness requirements. Finally, the experimental results show that significant performance improvement is achieved compared to common manual loop shaping methods. In addition, increased performance demands for new imaging systems are fulfilled.

Key words: System identification, robust control, model uncertainty, model validation, H$_\infty$, inertial stabilization

1. Introduction

In the last decades, increasing demands related to higher target detection and tracking range have increased the importance of good inertial stabilization and precise pointing-tracking performance of imaging systems on mobile platforms. Therefore, good disturbance rejection is becoming more essential to minimize the effects of vibrations and platform motions to sensor line-of-sight (LOS). Similarly, more rapid and precise response is needed for new tracking-pointing purposes.

Typical control structure is composed of inner inertial stabilization loops and outer position or tracking loops as depicted in Figure 1. Inner stabilization loops are closed around fast gyroscope sensors; whereas, outer loops use relatively slow feedback signals based on image processing or sensor position and attitude estimation in the inertial frame. Clearly, accuracy of pointing and tracking is directly determined from inner loop performance.

Therefore, high performing stabilization loop is necessary for pointing, tracking, and sensor isolation purposes. Consequently, bandwidth of the stabilization loop has to be increased while maintaining sufficient loop stability. However, recent performance demands require that target bandwidth and flexible dynamics are close. If low-cost micro-electro-mechanical systems (MEMS) gyroscopes are used, time delay of the sensors
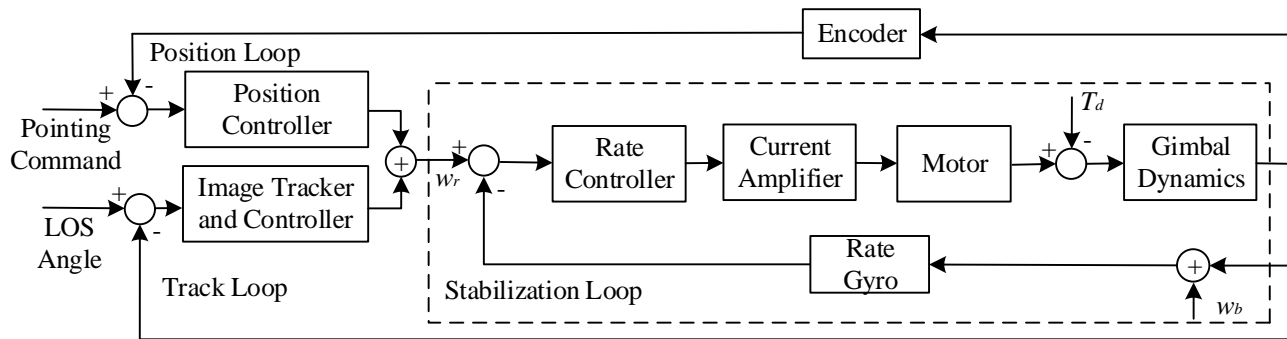
*Correspondence: mbaskin@aselsan.com.tr

Figure 1. Control structure of a typical imaging system.

becomes a major limiting factor for achievable bandwidth. This is also valid for the gimbaled system considered in this study. Traditional manual loop shaping methods select target bandwidth in the dominant rigid body region where the effects of flexible modes and time delay are small. In either case, model based control methods are needed to enlarge the bandwidth beyond common techniques. Among all, robust control methods can be more effective if high bandwidth and certain robustness should be satisfied simultaneously.

In traditional design techniques, feedback controller is often designed directly based on frequency response functions (FRF). These controllers originate from standard double-proportional-integral (PI) controller. Sometimes, notch filters are added to guarantee robust stability. Generally, to increase the stabilization loop performance two strategies are followed. In the first one, the disturbances are estimated by an observer, and their effects are compensated through feedforward path of the observer. $\mathcal{H}_\infty$-based robust disturbance observer control in [1] has been used recently. Different loop shaping methods to achieve desired loop bandwidth constitute the second strategy. General $\mathcal{H}_2$ and $\mathcal{H}_\infty$-norm optimization based mixed sensitivity designs in [2] are sometimes preferred since they are convenient loop shaping methods. Moreover, to meet some robustness requirements μ synthesis [2] and robust PI controller design [3] techniques are reported. In this paper, robust control type problem is considered since a finite order linear model is an approximation of the true model. In this respect, finite number of available states in the model to represent many resonance modes and time delay result in modeling errors. In addition, parasitic nonlinearities such as friction and nonlinear damping may exist in the true system, and all these errors should be addressed accurately. However, the main difficulty is to construct an uncertain model set which encompasses the model errors and facilitates high performance robust control for all possible plants in this set. This model set should be structured suitably to enable nonconservative robust control synthesis.

Standard additive and multiplicative uncertainty structures used in [2] generally fail to give similar performance for all candidate models in the set and may lead to conservative control design. In this respect, coprime factor based dual-Youla-Kucera uncertainty structure selection reduces conservatism in the design [4]. In addition, specific coprime factors for the nominal model and the controller enable connection of system identification and robust control. In the system identification step, robust control criterion is minimized jointly during successive nominal model and uncertainty computations [5]. Resulting robust-control-relevant model set enables a nonconservative control design and gives high performance for all candidate models unlike separate identification and control design techniques [2, 6].

Moreover, model validation based uncertainty modeling is used to determine the uncertainty bound. Model validation methods, where the nominal model residual is all attributed to uncertainty, may lead to overly

conservative design as applied in [2]. If all residual is attributed to additive disturbance, resulting control design may cause instability [6]. Therefore, model validation method suggested in [7] is used to obtain more accurate model set.

Contribution of this paper can be summarized as follows. In this paper, first implementation of combined system identification and robust control for a gimbaled platform is discussed. Resulting robust-control-relevant model set addresses two essential points. Firstly, for all plants in the model set similar high performance is achieved. Secondly, resulting tight model set significantly reduces conservatism in robust controller synthesis. In these aspects, significant contribution to previous works for inertial stabilization problem is made. Moreover, to the authors' knowledge, model validation based uncertainty modeling, and skewed-μ synthesis were not applied to any other gimbaled imaging system previously. However, these methods are important to construct accurate model set and to achieve high performance.

The outline of this paper can be summarized as follows. Firstly, combined system identification and robust control framework is reviewed. Secondly, resulting system identification problem is introduced. Next, construction of model set is summarized. Model validation based uncertainty modeling and skewed-μ synthesis based robust control design method are reviewed. After that, application of this methods to gimbal platform is reported. To visualize the performance improvement compared to common controller choices, different design and test results are illustrated. Finally, paper is finished with conclusion section.

2. Problem formulation

In this section, robust-control-relevant identification problem is introduced. During formulation following notations are used. The notation P is used to denote any linear time invariant system which may represent the actual plant P_o, or the nominal model $\hat{P}$. Moreover, $\mathcal{P}$ and C denote the model set and feedback controller, respectively. Finally, $\mathcal{H}_\infty$-norm based performance measure selection gives a control criterion $J(P,C)$ as

$$J(P,C) = \|WT(P,C)V\|_\infty, \tag{1}$$

where $W = \mathrm{diag}(W_y, W_u)$ and $V = \mathrm{diag}(V_2, V_1)$ are bistable weighting filters and transfer matrix $T(P,C)$ is the mapping defined as (2) corresponding to the feedback configuration in Figure 2.
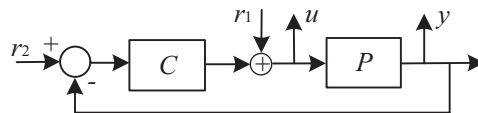

Figure 2. Feedback configuration for imaging system application.

$$T(P,C) : \begin{bmatrix} r_2 \\ r_1 \end{bmatrix} \rightarrow \begin{bmatrix} y \\ u \end{bmatrix} = \begin{bmatrix} P \\ I \end{bmatrix} (I + CP)^{-1} \begin{bmatrix} C & I \end{bmatrix} \tag{2}$$

The aim of the norm-based control design is to find an optimal controller C^{opt} such that following performance cost is minimized.

$$C^{\mathrm{opt}} = \arg \min_C J(P_o, C) \tag{3}$$

Since P_o is unknown, the optimal controller (3) can not be found. In order to represent the actual plant dynamics accurately, a model set $\mathcal{P}$ is constructed such that

$$P_o \in \mathcal{P}. \tag{4}$$

Then, the worst-case performance for this model set $\mathcal{P}$ is defined as

$$J_{WC}(\mathcal{P}, C) = \sup_{P \in \mathcal{P}} J(P, C). \tag{5}$$

Robust control design aims to minimize this worst-case performance criterion.

$$C^{\mathrm{RP}} = \arg \min_C J_{WC}(\mathcal{P}, C) \tag{6}$$

Then, the following performance bound for the true plant P_o is the basis for joint identification and robust control [9].

$$J(P_o, C^{\mathrm{RP}}) \leqslant J_{WC}(\mathcal{P}, C^{\mathrm{RP}}) \tag{7}$$

The performance guaranteed by (7) depends on shape and size of the model set $\mathcal{P}$, and it is structured using upper linear fractional transformation (LFT) [13] as

$$\mathcal{P} = \left\{ P \mid P = \mathcal{F}_u(\hat{H}, \Delta_u), \Delta_u \in \mathbf{\Delta_u} \right\}. \tag{8}$$

$\hat{H}$, which is shown in Figure 3 essentially contains the nominal model $\hat{P}$ and the uncertainty structure. In addition, $\mathcal{H}_\infty$-norm-bounded perturbation $\Delta_u \in \mathbf{\Delta_u} \subseteq \mathcal{RH}_\infty$ in (9) is considered.

$$\mathbf{\Delta_u} = \{\Delta_u \in \mathcal{RH}_\infty \mid \|\Delta_u\|_\infty \leqslant \gamma\} \tag{9}$$
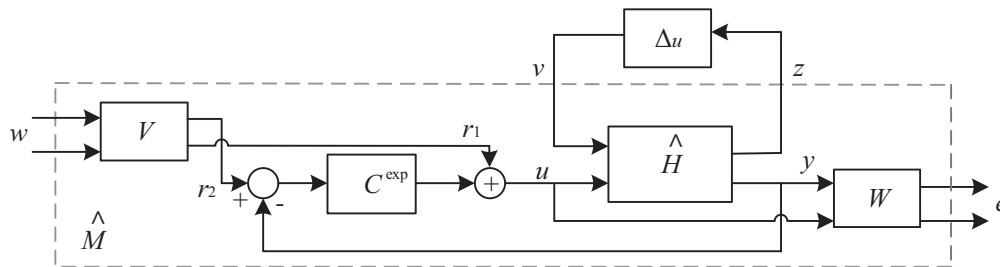

Figure 3. General control structure for worst-case performance evaluation.

Therefore, low complexity model set $\mathcal{P}$ which leads to nonconservative control design, and small performance bound (7) is needed. Specific coprime factor based approach introduced in [10] eventually satisfies these two requirements.

3. Robust-control-relevant identification
The minimization of performance bound (7) can not be solved explicitly. However, separate nominal model identification and uncertainty modeling step can be used jointly to reach approximate solution [5].

3.1. Uncertainty structure for robust control

Robust-control-relevant model set should give a small bound (7) for high robust performance. Therefore, following identification criterion selection is reasonable,

$$\min_{\mathcal{P}} J_{WC}(\mathcal{P}, C^{\mathrm{exp}}) \ , \ \ \text{subject to (4)} \tag{10}$$

where C^{exp} denotes the controller which stabilizes the system during identification experiment. If the distance between C^{exp} and C^{RP} is too large, (6) and (10) can be solved iteratively similar to the iterative identification method introduced in [12]. Since the iterative identification and control using model set gives monotonically improved performance, the effect of initial controller usage C^{exp} instead of C^{RP} is greatly reduced after several iterations [11]. In this respect, it is assumed that initial controller C^{exp} and C^{RP} are close, and only one iteration is performed.

The uncertainty structure selection is important to simplify the minimization of (10). Let the LFT description of $\mathcal{P}$ is augmented with weights and C^{exp} as in Figure 3.

Then, the worst-case performance evaluation of this structure leads to following equation where $\hat{M}$ is partitioned suitably as $\hat{M} = \left[\begin{array}{c|c} \hat{M}_{11} & \hat{M}_{12} \\ \hline \hat{M}_{21} & \hat{M}_{22} \end{array}\right]$.

$$J_{WC}(\mathcal{P}, C^{\mathrm{exp}}) = \sup_{\Delta_u \in \mathbf{\Delta_u}} \|\mathcal{F}_u(\hat{M}, \Delta_u)\|_\infty = \sup_{\Delta_u \in \mathbf{\Delta_u}} \|\hat{M}_{22} + \hat{M}_{21}\Delta_u(I - \hat{M}_{11}\Delta_u)^{-1}\hat{M}_{12}\|_\infty \tag{11}$$

For a model set constructed with plants that are stabilized by C^{exp}, (11) can be simplified, and bounded performance can be obtained. This is achieved by using dual-Youla-Kucera uncertainty structure (12), which requires coprime factorization approach. Right coprime factorization (RCF) of $\hat{P}$ is denoted by the pair $\{\hat{N}, \hat{D}\}$ if $\hat{D}$ is invertible, $\hat{N}, \hat{D} \in \mathcal{RH}_\infty$, $\hat{P} = \hat{N}\hat{D}^{-1}$, and $\exists X_r, Y_r \in \mathcal{RH}_\infty$ satisfying Bezout identity $X_r\hat{D} + Y_r\hat{N} = I$. Similarly, it is assumed that the stabilizing controller C^{exp} has a RCF $\{N_c, D_c\}$.

$$\mathcal{P}^{\mathrm{DY}} = \left\{P \mid P = (\hat{N} + D_c\Delta_u)(\hat{D} - N_c\Delta_u)^{-1}, \Delta_u \in \mathbf{\Delta_u}\right\} \tag{12}$$

Therefore, this structure has a LFT representation (13), and upper LFT of it gives the model set (12).

$$\hat{H}^{\mathrm{DY}} = \left[\begin{array}{c|c} \hat{D}^{-1}N_c & \hat{D}^{-1} \\ \hline \hat{P}N_c + D_c & \hat{P} \end{array}\right] \tag{13}$$

Evaluation of $\hat{H}^{\mathrm{DY}}$ in the feedback connection in Figure 3 gives a LFT representation (14).

$$\hat{M}^{\mathrm{DY}}(\hat{P}, C^{\mathrm{exp}}) = \left[\begin{array}{c|c} 0 & (\hat{D} + C^{\mathrm{exp}}\hat{N})^{-1} \begin{bmatrix} C^{\mathrm{exp}} & I \end{bmatrix} V \\ \hline W \begin{bmatrix} D_c \\ -N_c \end{bmatrix} & WT(\hat{P}, C^{\mathrm{exp}})V \end{array}\right] \tag{14}$$

Therefore, worst-case performance (10) reduces to an affine function in Δ_u and becomes bounded.

$$J_{WC}(\mathcal{P}^{\mathrm{DY}}, C^{\mathrm{exp}}) = \sup_{\Delta_u \in \mathbf{\Delta_u}} \|\hat{M}_{22} + \hat{M}_{21}\Delta_u\hat{M}_{12}\|_\infty \tag{15}$$

Even if bounded performance is reached, the minimization of (15) is not clear due to existence of frequency dependent $\hat{M}_{21}$ and $\hat{M}_{12}$ terms. This can be further simplified in the next sections by selecting specific coprime factorization of $C^{\exp}$ [11].

3.2. Nominal model identification

Minimization of (10) is achieved by first identifying nominal model $\hat{P}$ according to certain criteria, followed by uncertainty modeling step. Therefore, control-relevant nominal modeling requires tight model set such that designed and achieved performance are close. The triangle equality is the basis of the nominal model identification criterion [12].

$$J(P_o, C) \leq J(\hat{P}, C) + \|W(T(P_o, C) - T(\hat{P}, C))V\|_\infty \tag{16}$$

The first term on the right is related to model based control design, whereas the second term corresponds to performance degradation term since the controller C is designed for $\hat{P}$ instead of P_o. Therefore, the nominal model identification aims to minimize this performance degradation term when evaluated for $C^{\exp}$ which is the controller used during identification experiment.

$$\min_{\hat{P}} \|W(T(P_o, C^{\exp}) - T(\hat{P}, C^{\exp}))V\|_\infty \tag{17}$$

Dual-Youla–Kucera based uncertainty structure requires coprime factors of $\hat{P}$. In fact, specific coprime factorization introduced in [10] connects nominal model identification (17) and identification of these coprime factors.

Let $\{\tilde{N}_e, \tilde{D}_e\}$ be a LCF of $[C^{\exp}V_2 \ V_1]$ with a co-inner numerator, i.e. $\tilde{N}_e\tilde{N}_e^* = I$, where $\tilde{N}_e = [\tilde{N}_{e,2} \ \tilde{N}_{e,1}]$. Then, robust-control-relevant identification criterion (17) reduces to robust-control-relevant coprime factor identification problem (18),

$$\min_{\hat{N}, \hat{D}} \|W\left(\begin{bmatrix} N_o \\ D_o \end{bmatrix} - \begin{bmatrix} \hat{N} \\ \hat{D} \end{bmatrix}\right)\tilde{N}_e\|_\infty \tag{18}$$

$$\text{subject to } \hat{N}, \hat{D} \in \mathcal{RH}_\infty$$

where $\{\hat{N}, \hat{D}\}$ and $\{N_o, D_o\}$ denote the coprime factors for $\hat{P}$ and P_o respectively, and they are defined according to (19) [10].

$$\begin{bmatrix} N \\ D \end{bmatrix} = \begin{bmatrix} P \\ I \end{bmatrix} (\tilde{D}_e + \tilde{N}_{e,2}V_2^{-1}P)^{-1} \tag{19}$$

Since $\tilde{N}_e$ is coinner that does not affect the $\mathcal{H}_\infty$-norm, it can be omitted from (18). Using the $\mathcal{H}_\infty$ norm definition at a discrete frequency grid and introducing appropriate parametrization θ for $[\hat{N}^T(\theta) \ \hat{D}^T(\theta)]^T$, the problem can be reduced to (20).

$$\min_{\theta} \ \max_{w_i \in \Omega} \bar{\sigma}\left(W\left(\begin{bmatrix} N_o(w_i) \\ D_o(w_i) \end{bmatrix} - \begin{bmatrix} \hat{N}(\theta, w_i) \\ \hat{D}(\theta, w_i) \end{bmatrix}\right)\right) \tag{20}$$

$$\text{subject to } \hat{N}, \hat{D} \in \mathcal{RH}_\infty$$

The minimization of (20) is converted to linear least squares problem by using Lawson's algorithm for ℓ_∞ approximation and by applying Sanathanan–Koerner (SK) iterations. Instead of using standard monomials for θ, choosing orthonormal polynomials with respect to data-dependent inner product [14] improves the numerical conditioning of the problem. Subsequent SK and Gauss–Newton iterations give accurate parametric coprime factors as discussed in [9] in a detailed way.

4. Robust-control-relevant model set

In this section, the final step of the robust-control-relevant identification is discussed. Firstly, (W_u, W_y)-normalized coprime factorization satisfying (21) of C^{exp} is needed.

$$\begin{bmatrix} W_u N_c \\ W_y D_c \end{bmatrix}^* \begin{bmatrix} W_u N_c \\ W_y D_c \end{bmatrix} = I \tag{21}$$

Finally, the robust-control-relevant model set $\mathcal{P}^{\mathrm{RCR}}$ is derived from dual-Youla uncertainty structure (12) with a specific choice of $\{\hat{N}, \hat{D}\}$ and $\{N_c, D_c\}$ as

$$\mathcal{P}^{\mathrm{RCR}} = \left\{ P \mid P \in \mathcal{P}^{\mathrm{DY}}, \{\hat{N}, \hat{D}\} \text{ satisfies } (19) \,,\, \{N_c, D_c\} \text{ satisfies } (21) \right\}. \tag{22}$$

The LFT representation given in (14) for the feedback connection in Figure 3 is now updated for these particular coprime factors as

$$\hat{M}^{\mathrm{RCR}} = \left[\begin{array}{c|c} 0 & \begin{bmatrix} \tilde{N}_{e,2} & \tilde{N}_{e,1} \end{bmatrix} \\ \hline \begin{bmatrix} W_y D_c \\ -W_u N_c \end{bmatrix} & WT(\hat{P}, C^{\mathrm{exp}})V \end{array} \right]. \tag{23}$$

Then, the worst-case performance shown in (11) is evaluated for $\mathcal{P}^{\mathrm{RCR}}$.

$$J_{WC}(\mathcal{P}^{\mathrm{RCR}}, C^{\mathrm{exp}}) = \sup_{\Delta_u \in \mathbf{\Delta_u}} \|M_{22}^{\mathrm{RCR}} + M_{21}^{\mathrm{RCR}} \Delta_u M_{12}^{\mathrm{RCR}}\|_\infty \leqslant \|M_{22}^{\mathrm{RCR}}\|_\infty + \sup_{\Delta_u \in \mathbf{\Delta_u}} \|M_{21}^{\mathrm{RCR}} \Delta_u M_{12}^{\mathrm{RCR}}\|_\infty \tag{24}$$

$$= J(\hat{P}, C^{\mathrm{exp}}) + \gamma \tag{25}$$

Norm preserving properties of M_{12}^{RCR} and M_{21}^{RCR} give the result (25) [11]. It shows that uncertainty bound γ directly affects the worst-case performance. When the robust-control-relevant model set (22) is used, nominal model identification and uncertainty modeling procedure to determine γ together minimize the criterion (10).

5. Model validation

The aim of the model validation is to check the consistency of an uncertain model with measured data. Model residuals should be partitioned correctly between additive disturbance term at the system output and perturbation term. Allocating larger portions of residuals to disturbance may result in poor performance and instability; whereas, allocating larger portions to perturbation may result in overly conservative design. To address this ill-posedness of model validation problem, an estimator is suggested in [7, 8] for a disturbance model. When the disturbance model and the input-output data sets are available, model validation problem can be solved by using the generalization of structured singular value for implicit LFTs. The problem is briefly introduced by following similar strategy followed in [7, 8].

5.1. Problem formulation

The model validation problem is considered in the framework depicted in Figure 4, where $M_o \in \mathcal{RH}_\infty^{n_x \times n_w}$, x_m, d_{true} and w denote the actual system, measured output, disturbance term, and manipulated input, respectively. Consequently, the true system is governed by (26).
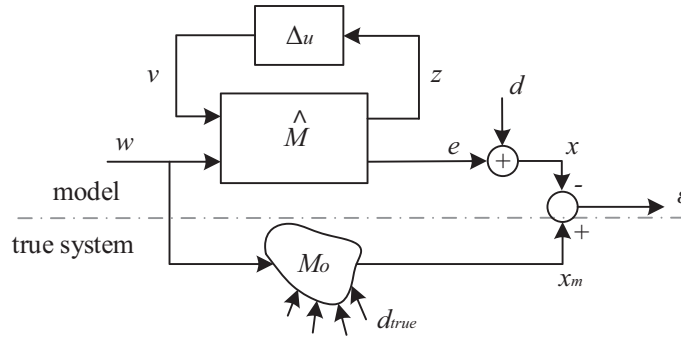

Figure 4. Model validation framework.

$$x_m = M_o w + d_{\text{true}} \tag{26}$$

Let $\hat{M} \in \mathcal{RH}_\infty^{(n_z+n_x)\times(n_v+n_w)}$ be the interconnection structure including the controller, nominal model, uncertainty structure and weighting functions, and x and d denote the uncertain model output and disturbance model. Then, the uncertain model is defined as

$$x = \mathcal{F}_u(\hat{M}, \Delta_u)w + d, \tag{27}$$

where the $\mathcal{H}_\infty$-norm bounded perturbation block $\mathbf{\Delta_u}$ is specified as in [13].

$$\mathbf{\Delta_u^c} = \{\text{diag}(\delta_1 I_{r_1}, ..., \delta_s I_{r_s}, \Delta_{S+1}, ..., \Delta_{S+F}) : \delta_i \in \mathbb{C}, \Delta_{S+j} \in \mathbb{C}^{n_{v_j} \times n_{z_j}}, 1 \leqslant i \leqslant S, 1 \leqslant j \leqslant F\}$$
$$\mathbf{\Delta_u} = \{\Delta_u \in \mathbf{\Delta_u^c} : \bar{\sigma}(\Delta_u) \leqslant \gamma\} \tag{28}$$

Let the measured signals w and x_m have discrete Fourier transform (DFT) $W(w_i)$ and $X_m(w_i)$ on a DFT grid $w_i \in \Omega$, and Ω^{val} is the part of Ω where $W(w_i) \neq 0$. Then, the uncertain model residual is equal to $E(w_i) = X_m(w_i) - X(w_i)$, where $X(w_i)$ is the DFT of $x(t)$. Moreover, let $D(w_i)$ denote the DFT of $d(t)$, and let it belong to certain set $\mathbf{D}(w_i)$. Then, model validation problem requires two problem definition from [7].

Frequency domain model validation decision problem (FDMVDP): It is assumed that the uncertain model (27), norm bound $\gamma(w_i) = \bar{\sigma}(\Delta_u(w_i))$, measurements $W(w_i)$ and $X_m(w_i)$ on $w_i \in \Omega^{\text{val}}$ and disturbance $D(w_i) \in \mathbf{D}(w_i)$ are known. Then, FDMVDP determines whether the uncertain model reproduces the measured signal at frequency w_i, namely $E(w_i) = 0$.

Frequency domain model validation optimization problem (FDMVOP): It is assumed that the uncertain model (27), measurements $W(w_i)$ and $X_m(w_i)$ on $w_i \in \Omega^{\text{val}}$ and disturbance $D(w_i) \in \mathbf{D}(w_i)$ are known. Then, FDMVOP aims to find minimum $\gamma(w_i)$ such that $E(w_i) = 0$.

The disturbance model $D(w_i) \in \mathbf{D}(w_i)$ is obtained by approximating stochastic disturbances by deterministic models for each frequency $w_i \in \Omega^{\text{val}}$. In this study, an estimator suggested in [8] is followed. In the FDMVDP, the model is not invalidated if the corresponding structured singular value test is satisfied [8]. Therefore, FDMVOP can easily be solved by using bisection algorithm and applying invalidation test each time for a new $\gamma(w_i)$.

6. Robust controller synthesis

In this section, robust controller design method is reviewed for the determined uncertain model set $\mathcal{P}^{\text{dyn}}$. For the identified parametric uncertainty bound W_γ, the generalized plant (29) is obtained. Structured singular value synthesis (30) is used for this generalized structure depicted in Figure 5.

$$G = \left[\begin{array}{c|ccc} W_\gamma \hat{D}^{-1} N_c & 0 & W_\gamma \hat{D}^{-1} V_1 & W_\gamma \hat{D}^{-1} \\ \hline W_y (D_c + \hat{P} N_c) & 0 & W_y \hat{P} V_1 & W_y \hat{P} \\ 0 & 0 & W_u V_1 & W_u \\ \hline -(D_c + \hat{P} N_c) & V_2 & -\hat{P} V_1 & -\hat{P} \end{array} \right] \tag{29}$$

$$C^{\text{RP}} = \arg\min_C J_{WC}(\mathcal{P}, C) = \arg\min_C \sup_{w \in [0, 2\pi)} \mu_s \left(\mathcal{F}_l \left(G(e^{jw}), C(e^{jw}) \right) \right) \tag{30}$$
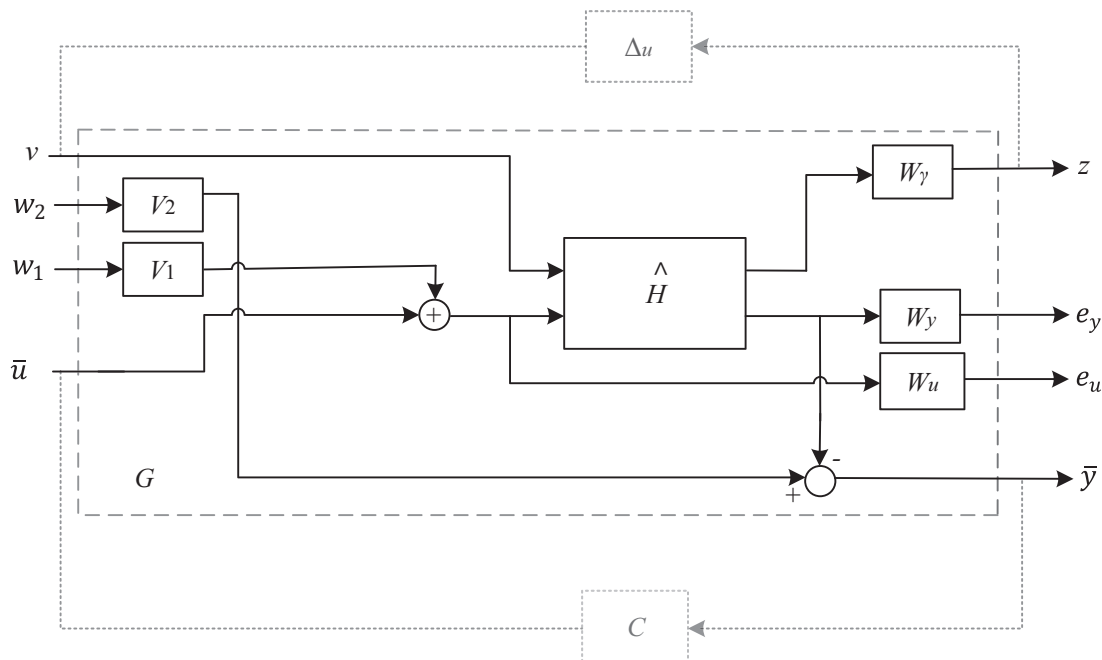

Figure 5. Generalized plant for robust controller synthesis.

Standard μ synthesis aims to optimize robustness and performance at the same time. Therefore, this method is not suitable to problems where the uncertainty is already determined and required robustness is known. For that reason, skewed-μ definition is used for $\bar{\Delta}$ as

$$\mu_{s,\bar{\Delta}} = \left(\min\{\bar{\sigma}(\Delta_t) \mid \bar{\Delta} \in \bar{\mathbf{\Delta}}, \ \det(I - M\bar{\Delta}) = 0\}\right)^{-1} \tag{31}$$

$$\bar{\mathbf{\Delta}} = \{\mathrm{diag}(\Delta_u, \Delta_t) \mid \bar{\sigma}(\Delta_u) \leq 1, \ \Delta_u \in \mathbf{\Delta_u}, \ \Delta_t \in \mathbf{\Delta_t}\}. \tag{32}$$

Solution method of skewed-μ synthesis is $D - K$ iterations as in the standard case. However, the aim of the $D - K$ iterations is slightly modified as $\min_{K,D} \|DU\hat{M}D^{-1}\|_\infty$ by introducing a new matrix $U = \mathrm{diag}(I_n, \frac{1}{\mu_s}I_{n_p})$, which is updated at each iteration.

7. Inertially stabilized gimbal platform system identification and robust control

Control-relevant identification and robust controller design methods discussed in the previous sections are now applied to the gimbal platform shown in Figure 6. Even if it is a two-axis platform, both gimbals are designed symmetrically to decouple the axes approximately in the inertial frame. Moreover, no multivariable resonance is observed during identification experiments. Therefore, separate SISO designs are preferred for each axis. In this paper, only elevation axis control problem is discussed.

Figure 6. Experimental gimbal platform.

7.1. Frequency response function identification

The frequency response functions (FRF) are derived by manipulating mapping (2) for Figure 2. During identification tests, signals r_1, u and y are measured, and r_1 excitation signal is applied and r_2 is kept at zero. Therefore, following equation is obtained where the DFTs of measured signals $\mathcal{R}_1$, $\mathcal{U}$, $\mathcal{Y} \in \mathbb{C}$.

$$\begin{bmatrix} \mathcal{Y} \\ \mathcal{U} \end{bmatrix} = \begin{bmatrix} P_o \\ 1 \end{bmatrix} (1 + C^{\mathrm{exp}} P_o)^{-1} \mathcal{R}_1 \tag{33}$$

Then, the estimation of $T(P_o, C^{\mathrm{exp}})$ is obtained as (34) on $\Omega^{\mathrm{id}} = \{w \mid w \in \Omega, \mathcal{R}_1 \neq 0\}$.

$$\tilde{T}(P_o, C^{\text{exp}}) = \begin{bmatrix} \mathcal{Y} \\ \mathcal{U} \end{bmatrix} \mathcal{R}_1^{-1} \begin{bmatrix} C^{\text{exp}} & 1 \end{bmatrix} \tag{34}$$

$$r_1 = \sum_k a_k \sin(w_k t + \phi_k) \tag{35}$$

Multisine input signals (35) are used to reduce the variance of estimate where $w_k \in \Omega^{\text{id}}$. Finally, the estimate of P_o is obtained by $\tilde{P}_o = \tilde{T}_{12}\tilde{T}_{22}^{-1}$ on Ω^{id} and depicted in Figure 7. Similarly, nonparametric estimate of $\{N_o, D_o\}$ on Ω^{id} is obtained by manipulating the equality between (17) and (18) as

$$\begin{bmatrix} \tilde{N}_o \\ \tilde{D}_o \end{bmatrix} = \tilde{T}(P_o, C^{\text{exp}})V\tilde{N}_e^*. \tag{36}$$
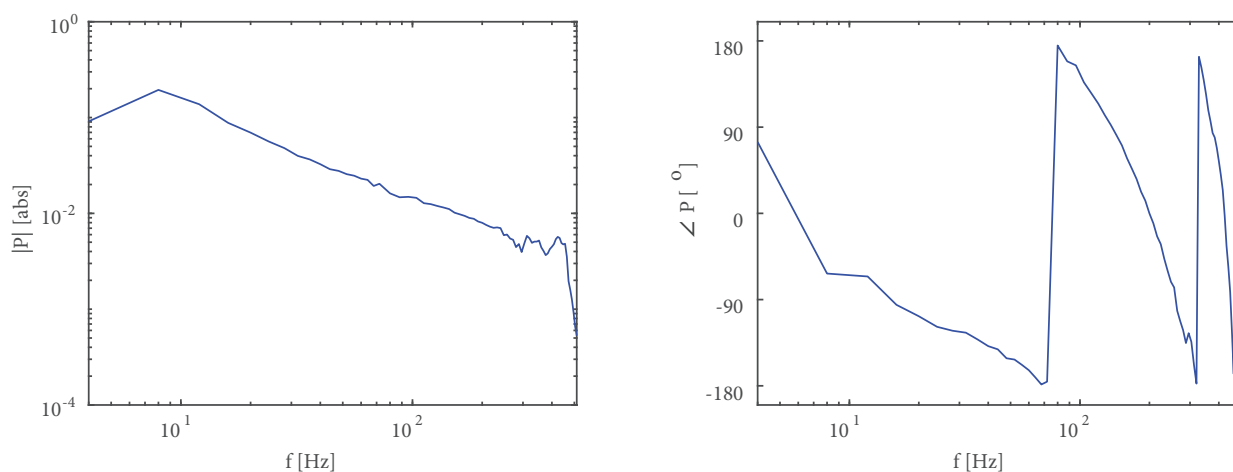
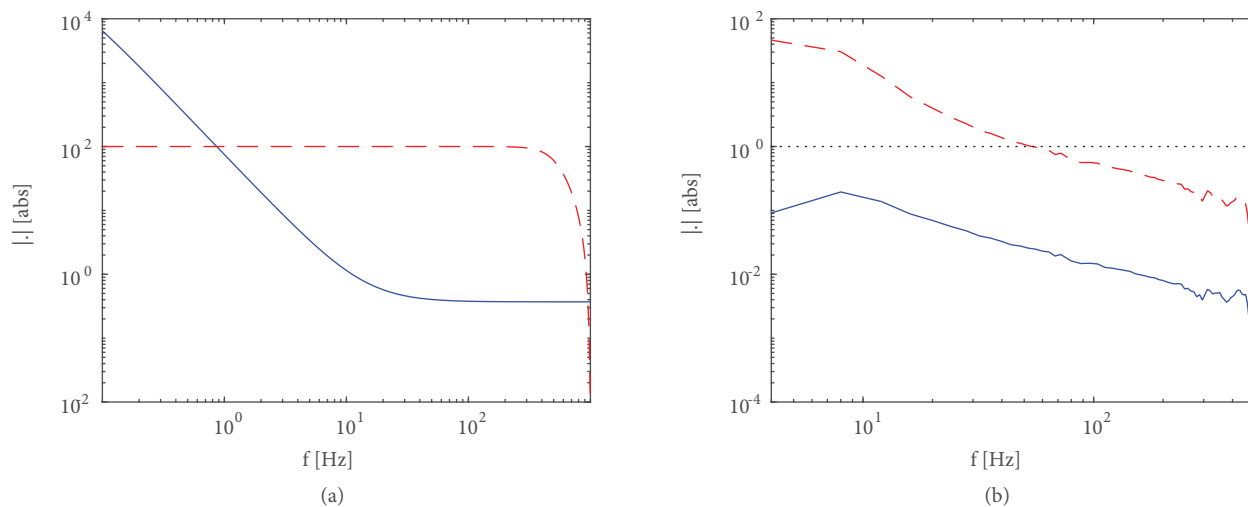

Figure 7. Identified frequency response function of $\tilde{P}_o$ on Ω^{id}.

In this paper, frequency grid Ω^{id} (37) is used during identification, and the data sets are obtained applying three different tests corresponding to different frequency ranges. Data sets are obtained with a sampling frquency of 2 kHz, and multisine input signals are periodic with a period of 1 second. Moreover, phases are selected according to Schröder rule. Identification tests take nearly 900 seconds, which corresponds to 900-period input excitation which is essential to reduce the covariance estimate of the disturbance and to obtain accurate FRFs [7].

$$\Omega^{\text{id}} = 2\pi\{4, 8, 12, ..., 68\} \cup 2\pi\{72, 80, 88, ..., 256\} \cup 2\pi\{264, 272, 280, ..., 512\} \tag{37}$$

Weight determination: Firstly, standard double-PI controller C^{exp} with integral cut-off at $f_{bw}/5$ and $f_{bw}/3$ which gives approximately $f_{bw} = 25$ Hz bandwidth, $30°$ phase margin and 2.5 gain margin is designed based on an open loop FRF. The main motivation is to reach approximately 55 Hz bandwidth and satisfy certain robustness. In this paper, bandwidth refers to gain crossover frequency f_{bw}. Weighting functions are selected to shape the loop similar to method in [15]. The two-block problem considered in [15] is equivalent to four-block problem considered in this paper if weighting filters are selected as $W = \text{diag}(W_y, W_u) = \text{diag}(W_2, W_1^{-1})$

and $V = \text{diag}(V_2, V_1) = \text{diag}(W_2^{-1}, W_1)$ in (1). In this paper, this method is applied, and weighting filters are selected such that $W_2 P W_1$ has desired open loop shape of PC. Since $\hat{P}$ is not available yet, the estimate $\tilde{P}_o$ can be used directly. The weight selection method suggested in [16] for position loops is extended for stabilization (rate) loops. In this respect, W_1 is selected to have a double integrator for good disturbance rejection, and their cut-offs are at $f_{bw}/5$ and $f_{bw}/3$ as shown in Figure 8 where $f_{bw} = 55$ Hz. W_2 is selected to satisfy 0 slope around f_{bw} such that desired open loop shape has –1 slope in this region. Moreover, high frequency roll-off beyond $10 f_{bw}$ is also enforced with W_2. Finally, W_2 and shaped open loop $W_2 P W_1$ are depicted in Figure 8.

Figure 8. (a) Magnitude of weighting filters: W_1 (solid blue), W_2 (dashed red). (b) Magnitude of FRF estimate $\tilde{P}_o$ (solid blue), shaped system $W_2 \tilde{P}_o W_1$ (dashed red).
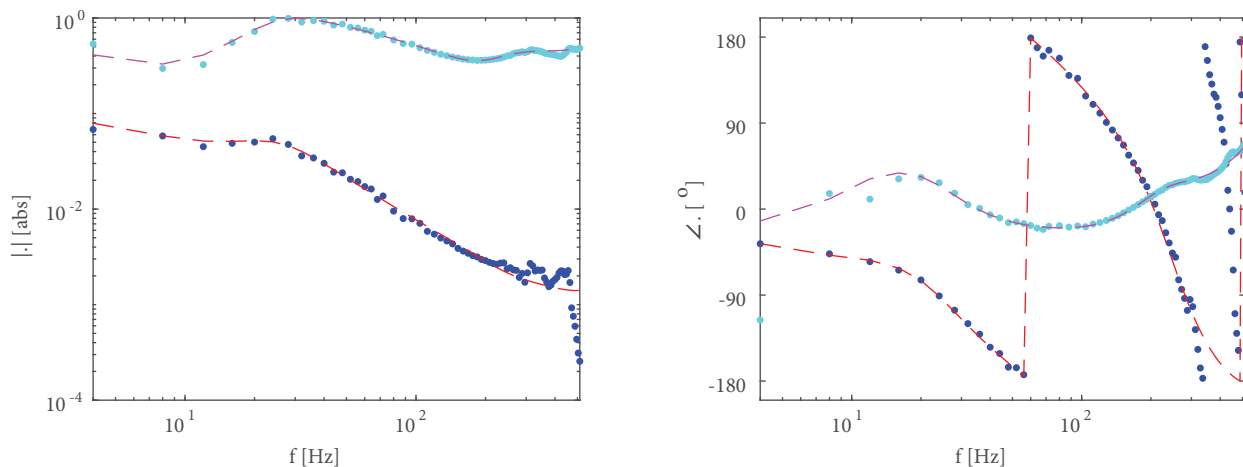
Coprime factorization: Nonparametric frequency response functions of $\tilde{N}_o$ and $\tilde{D}_o$ are obtained by using (36). As mentioned earlier, least squares fitting of these coprime factors using data-dependent orthonormal polynomials is obtained. These estimates are used in subsequent Gauss–Newton optimization step and results shown in Figure 9 are obtained.

7.2. Construction of model set

The identified coprime factorization is used to construct the robust-control-relevant model set $\mathcal{P}^{\text{RCR}}$ in (22). The uncertainty bound γ is estimated by applying model validation based uncertainty modeling. During this procedure, it is assumed that u is known exactly and it is omitted from (14) where $x = y$ and $w = [r_2 \ r_1]^T$ in the Figure 2. Since the validation procedure is applied by using measured variables, weighting filters are also omitted from (14), and following matrix is used.

$$\hat{M}^{\text{DY}}(\hat{P}, C^{\text{exp}}) = \left[\begin{array}{c|c} 0 & (\hat{D} + C^{\text{exp}}\hat{N})^{-1} \begin{bmatrix} C^{\text{exp}} & 1 \end{bmatrix} \\ \hline D_c & \hat{P}(1 + C^{\text{exp}}\hat{P})^{-1} \begin{bmatrix} C^{\text{exp}} & 1 \end{bmatrix} \end{array} \right] \tag{38}$$

Data sets are collected under different operating conditions by modifying excitation signal (35) as following.

Figure 9. Coprime factors: nonparametric N_o (blue dots), D_o (cyan dots), eleventh order parametric coprime factors $\hat{N}$ (dashed red), $\hat{D}$ (dashed magenta).

1. Data sets are collected with the same frequency components $w_i \in \Omega^{\mathrm{id}}$ and same phases ϕ_k as the signals used during identification experiments.

2. Data collected with the same frequency components $w_i \in \Omega^{\mathrm{id}}$ and with random phases ϕ_k. This set is used to investigate the effects of different phases around the resonances.

3. Data collected with different frequency components $w_i \in \Omega^{\mathrm{val}}$ (39), and $w_i \notin \Omega^{\mathrm{id}}$ and phases are selected according to Schröder rule. This set is used to investigate interpolation errors on the discrete frequency grid.

$$\Omega^{\mathrm{val}} = 2\pi\{6, 10, 14, ..., 70\} \cup 2\pi\{76, 84, 92, ..., 260\} \cup 2\pi\{268, 276, 284, ..., 516\} \tag{39}$$

$$\tilde{\gamma}(w_i) = \bar{\sigma}(\Delta_u(w_i)), w_i \in \Omega^{\mathrm{id}} \cup \Omega^{\mathrm{val}} \tag{40}$$

Different norm-bounds $\tilde{\gamma}(w_i)$ as defined by (40) are shown in Figure 10a. Then, the model uncertainty bound is obtained as $\gamma = \sup_{w_i \in \Omega^{\mathrm{id}} \cup \Omega^{\mathrm{val}}} \tilde{\gamma}(w_i) = 0.5967$, and bistable dynamic overbound W_γ is illustrated in Figure 10a.

After that, two model sets are constructed using static overbound γ and dynamic overbound W_γ as

$$\mathcal{P}^{\mathrm{sta}} = \{P \in \mathcal{P}^{\mathrm{RCR}} \mid \|\Delta_u\|_\infty \leqslant \gamma\}, \tag{41}$$

$$\mathcal{P}^{\mathrm{dyn}} = \{P \in \mathcal{P}^{\mathrm{RCR}} \mid \|\Delta_u W_\gamma^{-1}\|_\infty \leqslant 1\}. \tag{42}$$

Using tight dynamic overbound W_γ does not affect the performance bound (25); however, it has certain advantage. Mainly, it reduces possible conservatism compared to static overbound during controller synthesis since $\mathcal{P}^{\mathrm{dyn}} \in \mathcal{P}^{\mathrm{sta}}$ [5]. The resulting model sets are visualized using the method introduced in [17]. This method uses generalized structured singular value μ_g and standard μ to determine minimum and maximum gain of the uncertain model set, respectively. Resulting model sets are depicted in Figure 10b.

(a)

(b)
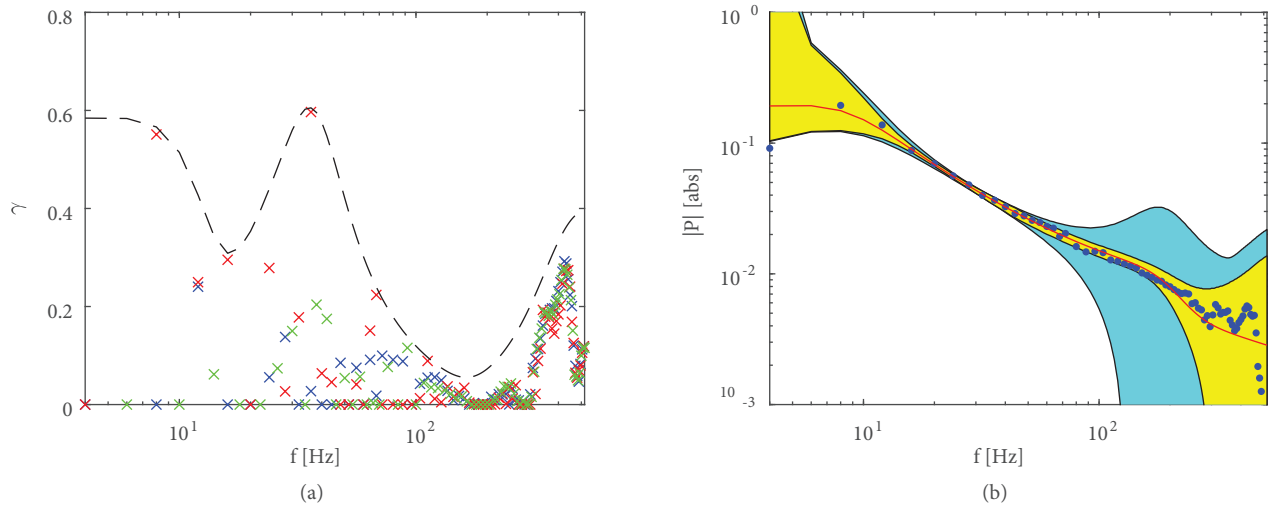
Figure 10. (a) Resulting model uncertainty norm bound $\tilde{\gamma}(w_i)$ on data sets: 1) on identification grid (blue $\times$), 2) with varying phases (red $\times$), 3) on validation grid (green $\times$), parametric overbound W_γ (dashed black). (b) Magnitudes of nonparametric estimate $\tilde{P}_o$ (blue dots), fifth order parametric nominal model $\hat{P}$ (solid red), model set $\mathcal{P}^{\mathrm{dyn}}$ (yellow shaded), $\mathcal{P}^{\mathrm{sta}}$ (cyan shaded).

7.3. Controller design and implementation

The uncertain model set $\mathcal{P}^{\mathrm{dyn}}$ is used to synthesize robust controller. In addition, using standard $\mathcal{H}_\infty$ optimization, C^{NP} is synthesized for nominal model $\hat{P}$. These three controllers are illustrated in Figure 11, and corresponding nominal and worst-case performances are given in Table .
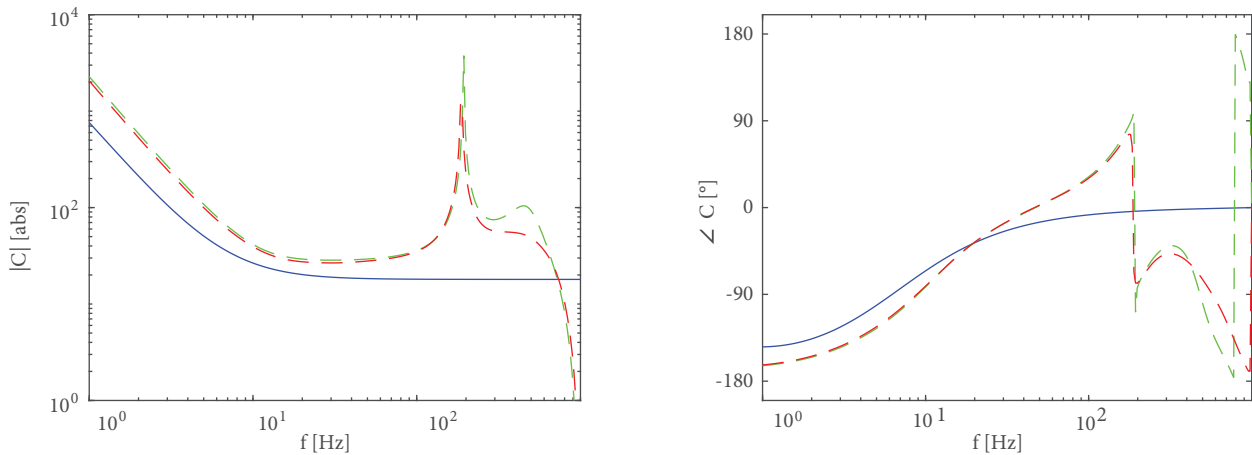
Figure 11. Bode plots: initial controller C^{exp} (solid blue), C^{NP} (dashed green), C^{RP} (dashed red).

Although, C^{NP} gives optimal performance for nominal model $\hat{P}$, it gives worse robust performance for $\mathcal{P}^{\mathrm{dyn}}$ than C^{RP}. Moreover, C^{RP} gives improved performance compared to C^{exp}, which is tuned using manual loop shaping rules. Smaller performance criterion indicates that achieved bandwidth is closer to desired one. Since $J(P,C) < 4$ indicates successful loop shape [15], C^{RP} has closer properties to desired loop shape. Table indicates that all candidate models in the uncertain model set give similar high performance for C^{RP} since J

Table . Robust-control-relevant identification and robust control synthesis results.

Controller	Minimized criterion	$J(\hat{P}, C)$	f_{bw}	$J_{WC}(\mathcal{P}^{\mathrm{dyn}}, C)$
C^{exp}	None (double-PI)	9.95	25.5	10.01
C^{NP}	$J(\hat{P}, C)$	3.44	36.8	4.24
C^{RP}	$J_{WC}(\mathcal{P}^{\mathrm{dyn}}, C)$	3.78	35	3.80

and J_{WC} are almost equal. In addition, robust-control-relevant set $\mathcal{P}^{\mathrm{dyn}}$ shown in Figure 10b is relatively tight and enable nonconservative controller synthesis.

Since C^{NP} turns out to be unstable and its worst-case performance is higher, only C^{RP} and C^{exp} are implemented. During implementation, instead of 46th-order controller, 10th-order reduced controller is implemented which leads to less than 0.01% worst-case performance decrement, which is insignificant.

Dominant angular rate disturbances to LOS can be illustrated with a sum of dominant sinusoids for small naval platform. For this paper, reference signal composed of sinusoids at 0.5, 1.5 and 3 Hz are generated. Tracking accuracy of this reference signal is used to investigate the performance of the stabilization loop. The command following properties are shown in Figure 12a. Since, LOS error is the main concern, corresponding cumulative power spectrum (CPS) of the LOS errors are depicted in Figure 12b. Since the error components are in the low frequency region, increasing the bandwidth gives better performance, and LOS error is decreased approximately by a factor of 2.5 with C^{RP}. Moreover, 50 μrad standard deviation of LOS error is good performance indicator for a typical two-axis gimbaled system. Consequently, C^{RP} gives significantly improved performance corresponding to C^{exp}.
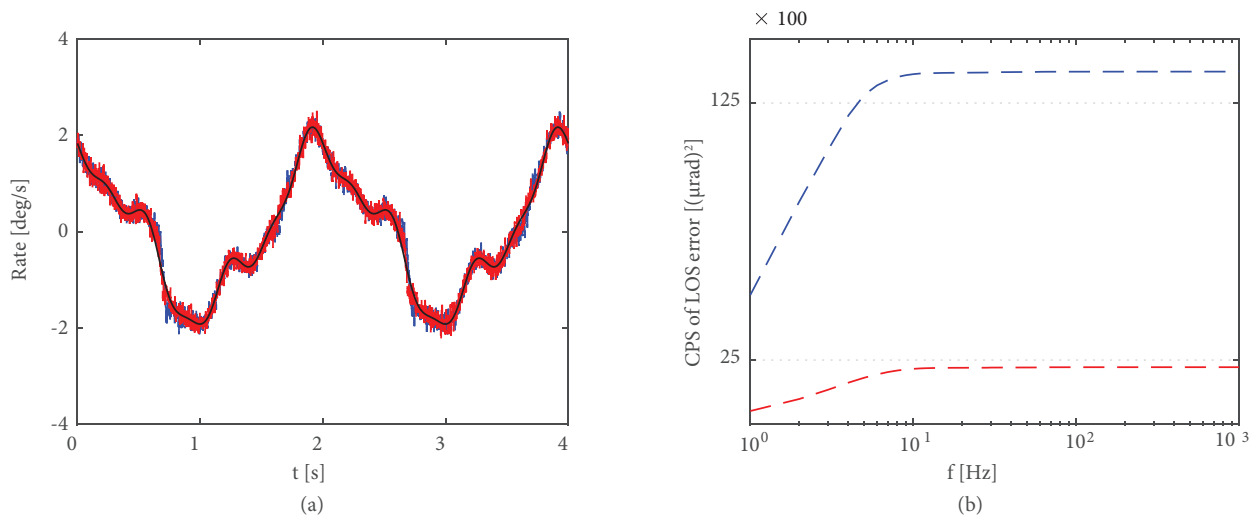
Figure 12. (a) Reference tracking: reference r_2 (solid black), system response with C^{exp} (dashed blue), C^{RP} (dashed red). (b) Cumulative power spectrum of LOS error: C^{exp} (dashed blue), C^{RP} (dashed red).

8. Conclusion

In this paper, combined system identification and robust control method were studied and implemented on a sample gimbaled system. Important performance improvement is achieved compared with a standard manual loop shaping method. The test results show that sufficient performance is achieved in terms of tolerable LOS

error for a typical two-axis gimbaled imaging system. Therefore, satisfactory design is provided considering both high disturbance rejection capability and accurate tracking and pointing purposes.

References

[1] Ali H, Ali A, Shaikh IUH. Disturbance observer based control of twin rotor aerodynamic system. Turkish Journal of Electrical Engineering & Computer Sciences 2020; 28 (4): 2213-2227. doi:10.3906/elk-1912-34

[2] Baskın M, Leblebicioğlu K. Robust control for line-of-sight stabilization of a two-axis gimbal system. Turkish Journal of Electrical Engineering & Computer Sciences 2017; 25 (5): 3839-3853. doi:10.3906/elk-1606-435

[3] Moaveni B, Khorshidi M. Robust speed controller design for induction motors based on IFOC and Kharitonov theorem. Turkish Journal of Electrical Engineering & Computer Sciences 2015; 23 (4): 1173-1186. doi:10.3906/elk-1306-22

[4] Oomen T, Bosgra O. Selecting uncertainty structures in identification for robust control with an automotive application. In: 16th IFAC Symposium on System Identification; Brussels, Belgium; 2012. pp. 601-606.

[5] Oomen T, van Herpen R, Quist S, van de Wal M, Bosgra O et al. Connecting system identification and robust control for next-generation motion control of a wafer stage. IEEE Transactions on Control Systems Technology 2014; 22 (1): 102-118. doi: 10.1109/TCST.2013.2245668

[6] Özdoğan G, Leblebicioğlu K. Frequency response function measurement and parametric SISO system modelling of a gyro-stabilized infrared electro optic gimbal system. Transactions of the Institute of Measurement and Control 2016; 38 (5): 512-528. doi:10.1177/0142331215596806

[7] Oomen T, Bosgra O. Well-posed model uncertainty estimation by design of validation experiments. In: 15th IFAC Symposium on System Identification; Saint-Malo, France; 2009. pp. 1199-1204.

[8] Oomen T, Bosgra O. Estimating disturbances and model uncertainty in model validation for robust control. In: 47th IEEE Conference on Decision and Control; Cancun, Mexico; 2008.

[9] Oomen T, Maarten S. Identification for robust control of complex systems: Algorithm and motion application. In: Lovera M (editor). Control-oriented Modelling and Identification: Theory and practice. Institution of Engineering and Technology, 2015, pp. 101-124.

[10] Oomen T, van Herpen R, Bosgra O. Robust-control-relevant coprime factor identification with application to model validation of a wafer stage. In: 15th IFAC Symposium on System Identification; Saint-Malo, France; 2009. pp. 1044-1049.

[11] Oomen T, Bosgra O. System identification for achieving robust performance. Automatica 2012; 48 (9): 1975-1987 doi:10.1016/j.automatica.2012.06.011

[12] Schrama RJP. Accurate identification for control: The necessity of an iterative scheme. IEEE Transactions on Automatic Control 1992; 37 (7): 991-994 doi:10.1109/9.148355

[13] Zhou K, Doyle JC, Glover K. Robust and optimal control. New Jersey, USA: Prentice Hall, 1996.

[14] van Herpen R, Oomen T, Bosgra O. Numerically reliable frequency-domain estimation of transfer functions: A computationally efficient methodology. In: 16th IFAC Symposium on System Identification; Brussels, Belgium; 2012. pp. 595-600.

[15] McFarlane D, Glover K. A loop-shaping design procedure using H_∞ synthesis. IEEE Transactions on Automatic Control 1992; 37 (6): 759-769 doi:10.1109/9.256330

[16] Steinbuch M, Norg ML. Advanced motion control: An industrial perspective. European Journal of Control 1998; 4 (4): 278-293 doi:10.1016/S0947-3580(98)70121-9

[17] Oomen T, Quist S, van Herpen R, Bosgra O. Identification and visualization of robust-control-relevant model sets with application to an industrial wafer stage. In:49th IEEE Conference on Decision and Control; Atlanta, GA, USA; 2010. pp. 5530-5535